Comput Mech (2008) 42:733–747
DOI 10.1007/s00466-008-0272-4

ORIGINAL PAPER

Null-field integral equation approach for free vibration analysis of circular plates with multiple circular holes

W. M. Lee · J. T. Chen

Received: 22 May 2007 / Accepted: 20 February 2008 / Published online: 29 April 2008

Abstract In this paper, a semi-analytical approach for the eigenproblem of circular plates with multiple circular holes is presented. Natural frequencies and modes are determined by employing the null-field integral formulation in conjunction with degenerate kernels, tensor rotation and Fourier series. In the proposed approach, all kernel functions are expanded into degenerate (separable) forms and all boundary densities are represented by using Fourier series. By uniformly collocating points on the real boundary and taking finite terms of Fourier series, a linear algebraic system can be constructed. The direct searching approach is adopted to determine the natural frequency through the singular value decomposition (SVD). After determining the unknown Fourier coefficients, the corresponding mode shape is obtained by using the boundary integral equations for domain points. The result of the annular plate, as a special case, is compared with the analytical solution to verify the validity of the present method. For the cases of circular plates with an eccentric hole or multiple circular holes, eigensolutions obtained by the present method are compared well with those of the existing approximate analytical method or finite element method (ABAQUS). Besides, the effect of eccentricity of the hole on the natural frequency and mode is also considered. Moreover, the inherent problem of spurious eigenvalue using the integral formulation is investigated and the SVD updating technique is adopted to suppress the occurrence of spurious eigenvalues. Excellent accuracy, fast rate of convergence and high computational efficiency are the main features of the present method thanks to the semi-analytical procedure.

Keywords Boundary integral equation · Null-field integral equation · Degenerate kernel · Fourier series · Vibration · Spurious eigenvalue · SVD updating technique

W. M. Lee
Department of Mechanical Engineering,
China Institute of Technology, Taipei, Taiwan

J. T. Chen (✉)
Department of Harbor and River Engineering,
National Taiwan Ocean University, P.O. Box 7-59,
Keelung 20224, Taiwan
e-mail: jtchen@mail.ntou.edu.tw

1 Introduction

Circular plates with multiple holes, including annular or annular-like plate, are often used to model mechanical elements and structural components for some applications. Compared with circular plates, these introduced holes result in significant changes in the natural frequency and mode shape. Free vibration analysis of this kind component is helpful to the work of mechanical design and flight control of the structure. As quoted by Leissa [19]: "the free vibrations of circular plates have been of practical and academic interest for at least a century and a half", most of research works have focused on the free vibration analysis of circular and annular plates [2,3,19,24–28]. However, only few studies have conducted the problem of plate with an eccentric hole [17] or multiple holes.

In the past, some analytical solutions [24] for natural frequencies of circular and annular plates were solved. Equations in frequency domain are obtained by substituting the general solution, which satisfies the governing equation of plates, into the boundary conditions. Since the analytical determination of natural frequencies requires the solution of transcendental functions (e.g., Bessel and modified Bessel functions), Vera et al. [25–27] obtained the desired eigenvalues by implementing the same procedure as [24] in the Maple V system and pointed out some inaccurate results in [18]. Recently some researchers intended to extend annular plate

[27,28] to the plate with an eccentric hole. Cheng et al. [11] encountered difficulty and resorted to finite element method (FEM) to implement the vibration analysis of annular-like plates due to the complicated expression for this kind of plate. Laura et al. [20] determined the natural frequencies of circular plate with an eccentric hole by using the Rayleigh–Ritz variational method where the coordinate function does not satisfy the natural boundary condition in the inner free edge. This approximate analytic solution can provide good results, but the accuracy of some results is insufficient after careful comparisons in this paper.

On the other hand, diverse numerical methods were resorted to the solution of plate problems, which include finite difference method (FDM), FEM and boundary element method (BEM). BEM has some advantages in comparison with domain discretization methods (FEM, FDM). The main gain is that the BEM reduces the dimension of the original problem by one, thus, the number of the introduced unknowns is much less than that of the traditional domain type methods. In addition, the domain mesh generation is not required, which is generally the most difficult and time-consuming task. For BEM applications to plate problems, readers may consult with the review article [21]. It is noted that improper integrals on the boundary should be handled particularly when the BEM is used. In the past, many researchers proposed several regularization techniques to deal with the singularity and hypersingularity. The determination of the Cauchy principal value (CPV) and the Hadamard principal value (HPV) in the singular and hypersingular integrals are critical issues in BEM/BIEM [4,23]. For the plate problem, it is more difficult to calculate the principal values since the kernels are involved with transcendental complex functions. In this paper, instead of using the previous concepts, the kernel function is recast into the degenerate kernel which is expanded into a series form on each side (interior and exterior) of the boundary by employing the addition theorem since the double-layer potential is discontinuous across the boundary. In reality, addition theorems are expansion formulae for the special functions (e.g., Bessel function, spherical harmonics, etc.) in a selected coordinate system [12]. Therefore, degenerate kernel, namely separable kernel, is a vital tool to study the perforated plate. Based on direct boundary integral formulation, Chen et al. [5–7] recently proposed the null-field integral equations in conjunction with degenerate kernels and Fourier series to solve boundary value problems with circular boundaries. By introducing the degenerate (separable) kernel, BIE involves nothing more than the linear algebra. Some applications were done in the static stress calculations of anti-plane [5] and plate problems [6]. The introduction of degenerate kernel in companion with Fourier series was proved to yield the exponential convergence [15] instead of the linear algebraic convergence in BEM.

This paper presents a semi-analytical approach to solve natural frequencies and modes of circular plates with multiple circular holes by using the null-field integral formulation in conjunction with degenerate kernels and Fourier series. A linear algebraic system is constructed by taking finite terms of Fourier series after uniformly collocating the null-field points exactly on the real boundary. By matching the boundary condition, the determinant of the influence matrix is zero to obtain the non-trivial eigensolution. The direct searching approach [16] is adopted to determine the natural frequency by using the singular value decomposition (SVD) [14]. After determining the Fourier coefficients, the corresponding mode shape of the circular plate with multiple circular holes is obtained by using the boundary integral equations for the domain point. For the plate problem, the slope (bending angle) and moment in the normal and tangential directions for the non-concentric domain are determined with care under the adaptive observer system. Therefore, the operator of transformation matrix for the slope and moment is adopted to deal with the problem for the non-concentric plate. Finally, the obtained result of the annular plate, as our special case, is compared with the analytical solution [18,25,27] to verify the validity of the present method. The results of the circular plate with an eccentric circular hole and/or multiple circular holes are compared with those of approximate analytical solution [20] and FEM using the ABAQUS [1] program to demonstrate the generality of the proposed method. The effect of eccentricity of the hole on the vibration characteristics of such plates subject to several boundary conditions is also addressed. Moreover, the inherent problem of spurious eigenvalues using BEM is investigated and the SVD updating technique [2] is employed to suppress the appearance of spurious eigenvalues.

2 Problem statement and boundary integral formulation

2.1 Problem statement of plate eigenproblems

The governing equation for the free flexural vibration of a uniform thin plate with non-overlapping circular holes as shown in Fig. 1 is written as follows:

$$\nabla^4 u(x) = \lambda^4 u(x), \quad x \in \Omega, \tag{1}$$

where ∇^4 is the biharmonic operator, u is the lateral displacement; $\lambda^4 = \omega^2 \rho_0 h/D$, λ is the frequency parameter; ω is the circular frequency; ρ_0 is the volume density; h is the plate thickness; $D = Eh^3/12(1-\nu^2)$ is the flexural rigidity of the plate; E denotes the Young's modulus; ν is the Poisson ratio of the elastic material; and Ω is the domain of the thin plate.

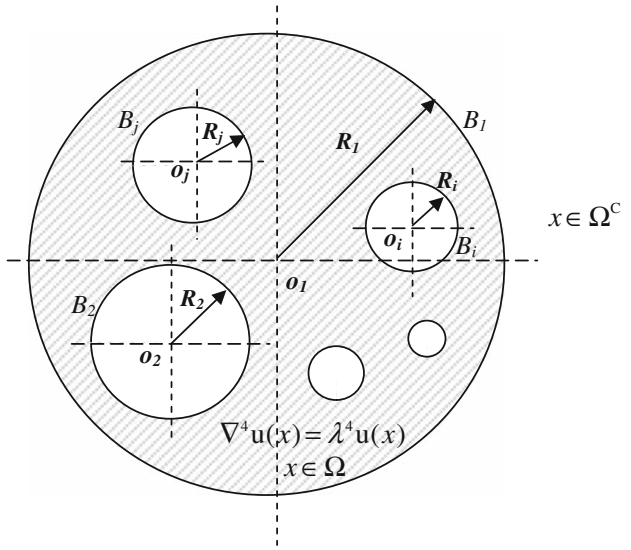

Fig. 1 Problem statement for an eigenproblem of a circular plate with multiple circular holes

2.2 Boundary integral equation for the domain point

The integral representation for the plate eigenproblem can be derived from the Rayleigh–Green identity [16] as follows:

$$u(x) = -\int_B U(s,x)\upsilon(s)dB(s) + \int_B \Theta(s,x)m(s)dB(s) - \int_B M(s,x)\theta(s)dB(s) + \int_B V(s,x)u(s)dB(s), \quad x \in \Omega, \tag{2}$$

$$\theta(x) = -\int_B U_\theta(s,x)\upsilon(s)dB(s) + \int_B \Theta_\theta(s,x)m(s)dB(s) - \int_B M_\theta(s,x)\theta(s)dB(s) + \int_B V_\theta(s,x)u(s)dB(s), \quad x \in \Omega, \tag{3}$$

$$m(x) = -\int_B U_m(s,x)\upsilon(s)dB(s) + \int_B \Theta_m(s,x)m(s)dB(s) - \int_B M_m(s,x)\theta(s)dB(s) + \int_B V_m(s,x)u(s)dB(s), \quad x \in \Omega, \tag{4}$$

$$\upsilon(x) = -\int_B U_\upsilon(s,x)\upsilon(s)dB(s) + \int_B \Theta_\upsilon(s,x)m(s)dB(s) - \int_B M_\upsilon(s,x)\theta(s)dB(s) + \int_B V_\upsilon(s,x)u(s)dB(s), \quad x \in \Omega, \tag{5}$$

where B is the boundary of the domain Ω, $u(x), \theta(x), m(x)$ and $\upsilon(x)$ are the displacement, slope, moment and shear force. The notations s and x mean the source and field points, respectively. The kernel functions $U(s,x)$, $\Theta(s,x)$, $M(s,x)$, $V(s,x)$, $U_\theta(s,x)$, $\Theta_\theta(s,x)$, $M_\theta(s,x)$, $V_\theta(s,x)$, $U_m(s,x)$, $\Theta_m(s,x)$, $M_m(s,x)$, $V_m(s,x)$, $U_\upsilon(s,x)$, $\Theta_\upsilon(s,x)$, $M_\upsilon(s,x)$ and $V_\upsilon(s,x)$ in Eqs. (2)–(5) can be expanded to degenerate kernels by separating the source and field points and will be elaborated later. The kernel function $U(s,x)$ in Eq. (2) is the fundamental solution which satisfies

$$\nabla^4 U(s,x) - \lambda^4 U(s,x) = \delta(s-x), \tag{6}$$

where $\delta(s-x)$ is the Dirac-delta function. Considering the two singular solutions ($Y_0(\lambda r)$ and $K_0(\lambda r)$, which are the zeroth-order of the second-kind Bessel and modified Bessel functions, respectively) [13] and the two regular solutions ($J_0(\lambda r)$ and $I_0(\lambda r)$, which are the zeroth-order of the first-kind Bessel and modified Bessel functions, respectively) in the fundamental solution, we have the complex-valued kernel,

$$U(s,x) = \frac{1}{8\lambda^2}\left[Y_0(\lambda r) + iJ_0(\lambda r) + \frac{2}{\pi}(K_0(\lambda r) + iI_0(\lambda r))\right], \tag{7}$$

where $r \equiv |s-x|$ and $i^2 = -1$. The other three kernels $\Theta(s,x)$, $M(s,x)$ and $V(s,x)$ in Eq. (2) can be obtained by applying the following slope, moment and effective shear operators defined by

$$K_\Theta = \frac{\partial(\cdot)}{\partial n}, \tag{8}$$

$$K_M = \nu\nabla^2(\cdot) + (1-\nu)\frac{\partial^2(\cdot)}{\partial n^2}, \tag{9}$$

$$K_V = \frac{\partial}{\partial n}\nabla^2(\cdot) + (1-\nu)\frac{\partial}{\partial t}\left[\frac{\partial}{\partial n}\left(\frac{\partial}{\partial t}(\cdot)\right)\right] \tag{10}$$

to the kernel $U(s,x)$ with respect to the source point, where $\partial/\partial n$ and $\partial/\partial t$ are the normal and tangential derivatives, respectively, and ∇^2 means the Laplacian operator. In the polar coordinate of (R,θ), the normal and tangential derivatives can be expressed by $\frac{\partial}{\partial R}$ and $\frac{1}{R}\frac{\partial}{\partial\theta}$, respectively and then the three kernel functions can be rewritten as:

$$\Theta(s,x) = K_{\Theta,s}(U(s,x)) = \frac{\partial U(s,x)}{\partial R}, \tag{11}$$

$$M(s,x) = K_{M,s}(U(s,x)) = \nu\nabla_s^2 U(s,x) + (1-\nu)\frac{\partial^2 U(s,x)}{\partial R^2}, \tag{12}$$

$$V(s,x) = K_{V,s}(U(s,x)) = \frac{\partial}{\partial R}\left(\nabla_s^2 U(s,x)\right) + (1-\nu)\left(\frac{1}{R}\right)\frac{\partial}{\partial\theta}\left[\frac{\partial}{\partial R}\left(\frac{1}{R}\frac{\partial U(s,x)}{\partial\theta}\right)\right]. \tag{13}$$

The expressions for $\theta(x)$, $m(x)$ and $v(x)$ in Eqs. (3)–(5), obtained by applying the operators in Eqs.(8)–(10) to $u(x)$ in Eq. (2) with respect to the field point $x(\rho,\phi)$, are

$$\theta(x) = K_{\Theta,x}(u(x)) = \frac{\partial u(x)}{\partial \rho}, \tag{14}$$

$$m(x) = K_{M,x}(u(x)) = \nu\nabla_x^2 u(x) + (1-\nu)\frac{\partial^2 u(x)}{\partial \rho^2}, \tag{15}$$

$$v(x) = K_{V,x}(u(x)) = \frac{\partial}{\partial \rho}\left(\nabla_x^2 u(x)\right) + (1-\nu)\left(\frac{1}{\rho}\right)\frac{\partial}{\partial \phi}\left[\frac{\partial}{\partial \rho}\left(\frac{1}{\rho}\frac{\partial u(x)}{\partial \phi}\right)\right]. \tag{16}$$

By the same way, the kernel functions $U_\theta(s,x)$, $\Theta_\theta(s,x)$, $M_\theta(s,x)$,$V_\theta(s,x)$, $U_m(s,x)$, $\Theta_m(s,x)$, $M_m(s,x)$,$V_m(s,x)$, $U_\upsilon(s,x)$, $\Theta_\upsilon(s,x)$, $M_\upsilon(s,x)$ and $V_\upsilon(s,x)$ can be obtained by applying the operators in Eqs.(8)–(10) respectively to the kernel functions U, Θ, M and V with respect to the field point $x(\rho,\phi)$.

2.3 Null-field integral equations

The null-field integral equations derived by collocating the field point outside the domain (including the boundary point if exterior degenerate kernels are properly adopted) are shown as follows:

$$0 = -\int_B U(s,x)\upsilon(s)dB(s) + \int_B \Theta(s,x)m(s)dB(s) - \int_B M(s,x)\theta(s)dB(s) + \int_B V(s,x)u(s)dB(s), \quad x \in \Omega^C \cup B, \tag{17}$$

$$0 = -\int_B U_\theta(s,x)\upsilon(s)dB(s) + \int_B \Theta_\theta(s,x)m(s)dB(s) - \int_B M_\theta(s,x)\theta(s)dB(s) + \int_B V_\theta(s,x)u(s)dB(s), \quad x \in \Omega^C \cup B, \tag{18}$$

$$0 = -\int_B U_m(s,x)\upsilon(s)dB(s) + \int_B \Theta_m(s,x)m(s)dB(s) - \int_B M_m(s,x)\theta(s)dB(s) + \int_B V_m(s,x)u(s)dB(s), \quad x \in \Omega^C \cup B, \tag{19}$$

$$0 = -\int_B U_\upsilon(s,x)\upsilon(s)dB(s) + \int_B \Theta_\upsilon(s,x)m(s)dB(s) - \int_B M_\upsilon(s,x)\theta(s)dB(s) + \int_B V_\upsilon(s,x)u(s)dB(s), \quad x \in \Omega^C \cup B, \tag{20}$$

where Ω^C is the complementary domain of Ω. Once kernel functions are expressed in proper degenerate forms, which will be described in the next subsection, the collocation points can be exactly located on the real boundary, that is $x \in \Omega^C \cup B$. Since the four equations of Eqs. (17)–(20) in the plate formulation are provided, there are 6 (C_2^4, $C(4,2)$ or $\binom{4}{2}$) options for choosing any two equations to solve the problems. Kernels in Eq. (20) involve higher-order derivatives, which may decrease both the convergence rate and computational efficiency. For the convergence rate, computational efficiency and treatment of the spurious eigenvalue, the Eqs. (17)–(19) are used to analyze the plate problem.

2.4 Degenerate kernels and Fourier series for boundary densities

In the polar coordinate, the field point and source point can be expressed as (ρ,ϕ) and (R,θ), respectively. By employing the separation technique for the source and field points, the kernel functions $U(s,x)$ are expanded in the series form as follows:

$$U: \begin{cases} U^I(s,x) = \dfrac{1}{8\lambda^2}\displaystyle\sum_{m=0}^{\infty}\varepsilon_m \left\{ J_m(\lambda\rho)[Y_m(\lambda R) + iJ_m(\lambda R)] + \dfrac{2}{\pi} I_m(\lambda\rho)[K_m(\lambda R) + i(-1)^m I_m(\lambda R)] \right\} \times cos\,[m\,(\theta-\phi)]\,, \rho < R, \\ U^E(s,x) = \dfrac{1}{8\lambda^2}\displaystyle\sum_{m=0}^{\infty}\varepsilon_m \left\{ J_m(\lambda R)[Y_m(\lambda\rho) + iJ_m(\lambda\rho)] + \dfrac{2}{\pi} I_m(\lambda R)[K_m(\lambda\rho) + i(-1)^m I_m(\lambda\rho)] \right\} \times cos\,[m\,(\theta-\phi)]\,, \rho \geq R, \end{cases} \tag{21}$$

where ε_m is the Neumann factor ($\varepsilon_m = 1, m = 0$; $\varepsilon_m = 2$, $m = 1,2,\ldots,\infty$) and the superscripts "I" and "E" denote the interior and exterior cases for degenerate kernel $U(s,x)$ to distinguish $\rho < R$ and $\rho > R$, respectively as shown in Fig. 2. The degenerate kernels $\Theta(s,x)$, $M(s,x)$ and $V(s,x)$ in the null-field boundary integral equations can be obtained by applying the operators of Eqs. (11)–(13) to the degenerate kernel $U(s,x)$ of Eq. (21).

In order to fully utilize the geometry of circular boundary, the displacement $u(s)$, slope $\theta(s)$, moment $m(s)$ and shear force $\upsilon(s)$ along the circular boundary in the null-field integral equations are expanded in terms of Fourier series, respectively, as shown below:

$$u(s) = c_0 + \sum_{n=1}^{M}(c_n\cos n\theta + d_n \sin n\theta), \quad s \in B, \tag{22}$$

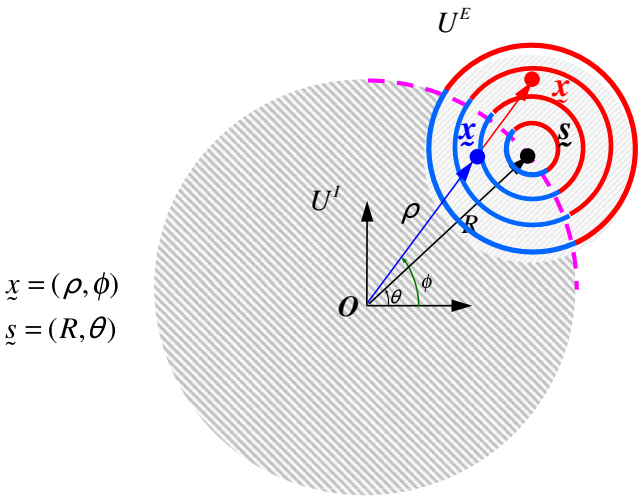

Fig. 2 Degenerate kernel for $U(s, x)$

$$\theta(s) = g_0 + \sum_{n=1}^{M} (g_n \cos n\theta + h_n \sin n\theta), \quad s \in B, \tag{23}$$

$$m(s) = a_0 + \sum_{n=1}^{M} (a_n \cos n\theta + b_n \sin n\theta), \quad s \in B, \tag{24}$$

$$\upsilon(s) = p_0 + \sum_{n=1}^{M} (p_n \cos n\theta + q_n \sin n\theta), \quad s \in B, \tag{25}$$

where $a_0, a_n, b_n, c_0, c_n, d_n, g_0, g_n, h_n, p_0, p_n$ and q_n are the Fourier coefficients and M is the number of Fourier series terms. The number of terms M in Fourier series for the circular boundaries can be, in general, different for each boundary circle. For simplicity, we used the same number of Fourier terms for each circular boundary. By using degenerated kernels, Fourier series and orthogonal property, all the improper integrals in Eqs. (17)–(20) can be transformed to series sum and then be calculated easily, since the potential across the boundary can be described in each side by using the degenerate kernel with series form. Successful experiences on Laplace problems [7], Helmholtz problems [8] and biharmonic problems [6] can be found.

3 Adaptive observer system and transformation of tensor components

3.1 Adaptive observer system

Consider a plate problem with circular boundaries as shown in Fig. 1. Since the direct boundary integral equations are frame indifferent (i.e., rule of objectivity), the origin of the observer system can be adaptively located on the center of the corresponding boundary contour under integration. Adaptive observer system is chosen to fully employ the circular property, which takes the full advantage of both Fourier series to represent boundary variables and degenerate-kernel expression in polar coordinate. Figure 3 shows the boundary integration for the circular boundaries in the adaptive observer system. The dummy variable in the circular contour integration is the angle (θ) instead of radial coordinate (R). By using the adaptive system, all the boundary integrals can be determined analytically free of principal value senses.

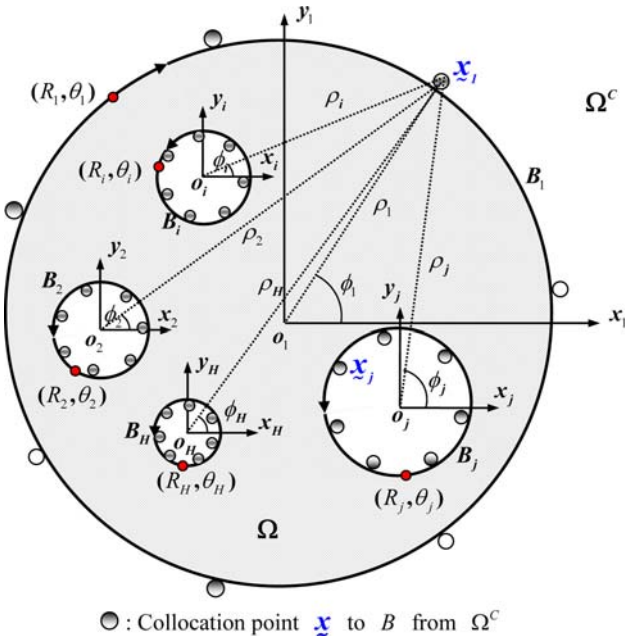

Fig. 3 Collocation point and boundary contour integration in the boundary integral equation in the adaptive observer system

3.2 Transformation of tensor components

Since the slope, moment and effective shear force are calculated in the plate problem, potential gradient or higher-order gradient need to be manipulated with care. For the non-concentric case, special care for determining the potential gradient should be taken as the source and field points locate on different circular boundaries. As shown in Fig. 4, the angle ϕ_i of the collocation point x_i is described in the center of the circle under integration and the angle ϕ_c is described in the center of the circle on which collocation point is located. According to the transformation of the component of tensor, we have [22]

$$\begin{bmatrix} (\cdot)_n \\ (\cdot)_t \end{bmatrix} = \begin{bmatrix} \cos(\delta) & \sin(\delta) \\ -\sin(\delta) & \cos(\delta) \end{bmatrix} \begin{bmatrix} (\cdot)_r \\ (\cdot)_\theta \end{bmatrix}, \tag{26}$$

$$\begin{bmatrix} (\cdot)_{nn} \\ (\cdot)_{nt} \end{bmatrix} = \begin{bmatrix} \cos^2(\delta) & \sin^2(\delta) & 2\sin(\delta)\cos(\delta) \\ -\sin(\delta)\cos(\delta) & \sin(\delta)\cos(\delta) & \cos^2(\delta) - \sin^2(\delta) \end{bmatrix} \begin{bmatrix} (\cdot)_{rr} \\ (\cdot)_{\theta\theta} \\ (\cdot)_{r\theta} \end{bmatrix}. \tag{27}$$

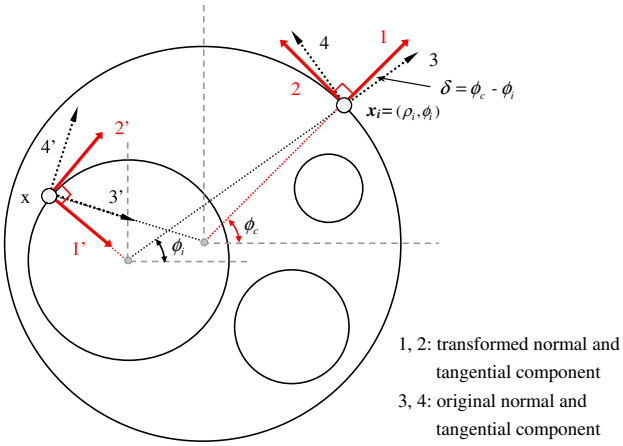

Fig. 4 Transformation of tensor components

Based on Eqs. (26) and (27), the operators in Eqs. (14) and (15) can be transformed as follows:

$$K_{\Theta}^{R} = \cos(\delta)\frac{\partial(\cdot)}{\partial n} + \sin(\delta)\frac{\partial(\cdot)}{\partial t}, \tag{28}$$

$$K_{M}^{R} = \left[\upsilon + (1-\nu)\sin^2(\delta)\right]\nabla^2(\cdot) + \cos(2\delta)(1-\nu)\frac{\partial^2(\cdot)}{\partial n^2} + \sin(2\delta)(1-\nu)\frac{\partial}{\partial n}\left(\frac{\partial(\cdot)}{\partial t}\right), \tag{29}$$

where $\delta = \phi_c - \phi_i$. When the angle ϕ_c equals to the angle ϕ_i or the angle difference δ equals to zero, Eqs. (28) and (29) are simplified to the Eqs. (14) and (15). Considering the non-concentric case, the degenerate kernels, $U_\theta(s,x)$, $\Theta_\theta(s,x)$, $M_\theta(s,x)$, $V_\theta(s,x)U_m(s,x)$, $\Theta_m(s,x)$ and $M_m(s,x)$ can be obtained by applying the operators of Eqs. (28)–(29) to the degenerate kernel $U(s,x)$, $\Theta(s,x)$, $M(s,x)$ and $V(s,x)$ with respect to the field point x.

4 Linear algebraic system

Consider the circular plate containing H non-overlapping circular holes centered at the position vector $\boldsymbol{o}_j$ ($j = 1, 2, \ldots, L$), ($L = 1 + H$ and $\boldsymbol{o}_1$ is the position vector for the center of the outer circular boundary), as shown in Fig. 3 in which R_j denotes the radius of the jth circular region, x_j is the collocation point on the jth circular boundary and B_j is the boundary of the jth circular hole. By uniformly collocating the N ($= 2M + 1$) points on each circular boundary in Eqs. (17)–(19), we have

$$0 = \sum_{j=1}^{L}\int_{B_j}\{-U(s,x)v(s) + \Theta(s,x)m(s) - M(s,x)\theta(s) + V(s,x)u(s)\}\,dB_j(s), \quad x \in B, \tag{30}$$

$$0 = \sum_{j=1}^{L}\int_{B_j}\{-U_\theta(s,x)v(s) + \Theta_\theta(s,x)m(s) - M_\theta(s,x)\theta(s) + V_\theta(s,x)u(s)\}\,dB_j(s), \quad x \in B. \tag{31}$$

$$0 = \sum_{j=1}^{L}\int_{B_j}\{-U_m(s,x)v(s) + \Theta_m(s,x)m(s) - M_m(s,x)\theta(s) + V_m(s,x)u(s)\}\,dB_j(s), \quad x \in B. \tag{32}$$

It must be noted that U, Θ, M, U_θ, Θ_θ and U_m are weakly singular, V, M_θ and Θ_m are singular and V_θ, M_m and V_m are hypersingular [29] since we select the null-field point on the boundary in the real computation. The main gain by using the degenerate kernel in the BIE is that singular integrals due to the kernels can be transformed to the series sum free of facing principal values. The selection of interior or exterior degenerate kernel depends on $\rho < R$ or $\rho > R$, respectively, according to the observer system. Besides, the path is counterclockwise for the outer circle; otherwise, it is clockwise. For the B_j circular boundary integrals, the degenerate kernels of $U(s,x)$, $\Theta(s,x)$, $M(s,x)$, $V(s,x)$, $U_\theta(s,x)$, $\Theta_\theta(s,x)$, $M_\theta(s,x)$ and $V_\theta(s,x)$ are utilized and boundary densities $u(s)$, $\theta(s)$, $m(s)$ and $v(s)$ along the circular boundary are substituted by using the Fourier series of Eqs. (22)–(25), respectively. In the B_j integration, the origin of the observer system is adaptively set to collocate at the center o_j from which the degenerate kernels and Fourier series are described. Considering the computational efficiency and the outer clamped and inner free boundary condition, we firstly chose Eqs. (30) and (31) to establish a linear algebraic system as follows:

$$\begin{bmatrix} -U^{11} & \Theta^{11} & -M^{12} & V^{12} & \cdots & -M^{1L} & V^{1L} \\ -U_\theta^{11} & \Theta_\theta^{11} & -M_\theta^{12} & V_\theta^{12} & \cdots & -M_\theta^{1L} & V_\theta^{1L} \\ -U^{21} & \Theta^{21} & -M^{22} & V^{22} & \cdots & -M^{2L} & V^{2L} \\ -U_\theta^{21} & \Theta_\theta^{21} & -M_\theta^{22} & V_\theta^{22} & \cdots & -M_\theta^{2L} & V_\theta^{2L} \\ \vdots & \vdots & \vdots & \vdots & \ddots & \vdots & \vdots \\ -U^{L1} & \Theta^{L1} & -M_\theta^{L2} & V^{L2} & \cdots & -M^{LL} & V^{LL} \\ -U_\theta^{L1} & \Theta_\theta^{L1} & -M_\theta^{L2} & V_\theta^{L2} & \cdots & -M_\theta^{LL} & V_\theta^{LL} \end{bmatrix} \begin{Bmatrix} v^1 \\ m^1 \\ \theta^2 \\ u^2 \\ \vdots \\ \theta^L \\ u^L \end{Bmatrix} = \begin{Bmatrix} 0 \\ 0 \\ 0 \\ 0 \\ \vdots \\ 0 \\ 0 \end{Bmatrix} \tag{33}$$

by using orthogonal property, where L denotes the number of circular boundaries (the superscript 1 denotes the outer boundary and the other number stands for the inner hole).

For brevity, a unified form $[U^{ij}]$ ($i = 1, 2, 3, \ldots, L$ and $j = 1, 2, 3, \ldots, L$) denote the response of $U(s, x)$ kernel on the ith circle due to the source on the jth circle. Otherwise, the same definition is for $[\Theta^{ij}]$, $[M^{ij}]$, $[V^{ij}]$, $[U_\theta^{ij}]$, $[\Theta_\theta^{ij}]$, $[M_\theta^{ij}]$ and $[V_\theta^{ij}]$ kernels. The explicit expressions for sub-vectors $[u^i]$, $[\theta^i]$,$[m^i]$ and $[v^i]$ can be described as follows:

$$u^i = \begin{Bmatrix} c_0^i \\ c_1^i \\ d_1^i \\ \vdots \\ c_M^i \\ d_M^i \end{Bmatrix} \quad \theta^i = \begin{Bmatrix} g_0^i \\ g_1^i \\ h_1^i \\ \vdots \\ g_M^i \\ h_M^i \end{Bmatrix} \quad m^i = \begin{Bmatrix} a_0^i \\ a_1^i \\ b_1^i \\ \vdots \\ a_M^i \\ b_M^i \end{Bmatrix} \quad v^i = \begin{Bmatrix} p_0^i \\ p_1^i \\ q_1^i \\ \vdots \\ p_M^i \\ q_M^i \end{Bmatrix}. \tag{34}$$

The explicit expressions for the sub-matrices of $[U^{ij}]$, $[\Theta^{ij}]$, $[M^{ij}]$, $[V^{ij}]$, $[U_\theta^{ij}]$, $[\Theta_\theta^{ij}]$, $[M_\theta^{ij}]$ and $[V_\theta^{ij}]$ can be written in the following form

$$K^{ij} = \begin{bmatrix} K_{0C}^{ij}(\rho_1, \phi_1) & K_{1C}^{ij}(\rho_1, \phi_1) & K_{1S}^{ij}(\rho_1, \phi_1) & \cdots & K_{MS}^{ij}(\rho_1, \phi_1) \\ K_{0C}^{ij}(\rho_2, \phi_2) & K_{1C}^{ij}(\rho_2, \phi_2) & K_{1S}^{ij}(\rho_2, \phi_2) & \cdots & K_{MS}^{ij}(\rho_2, \phi_2) \\ \vdots & \vdots & \vdots & & \vdots \\ \vdots & \vdots & \vdots & & \vdots \\ K_{0C}^{ij}(\rho_N, \phi_N) & K_{1C}^{ij}(\rho_N, \phi_N) & K_{1S}^{ij}(\rho_N, \phi_N) & \cdots & K_{MS}^{ij}(\rho_N, \phi_N) \end{bmatrix}_{N \times N}, \tag{35}$$

where K can be either one of U, Θ, M, V, U_θ, Θ_θ, M_θ and V_θ. The notations ϕ_k and $\rho_k (k = 1, 2, 3, \ldots, N)$ shown in Fig. 3 are the angle and radius of the kth collocation point on the ith circular boundary with respect to the center of the jth circular boundary (the origin of the observer system) and the element of the sub-matrices can be determined by

$$K_{nc}^{ij}(\rho_k, \phi_k) = \int_0^{2\pi} K(R_j, \theta_j; \rho_k, \phi_k) \cos(n\theta_j)(R_j d\theta_j), \quad n = 0, 1, 2, \ldots, M, \tag{36}$$

$$K_{ns}^{ij}(\rho_k, \phi_k) = \int_0^{2\pi} K(R_j, \theta_j; \rho_k, \phi_k) \sin(n\theta_j)(R_j d\theta_j), \quad n = 1, 2, \ldots, M \tag{37}$$

in which the selection of interior or exterior degenerate kernel depends on the position of collocation point with respective to the center of circle under integration as presented in Fig. 3. According to the direct-searching scheme, the eigenvalue can be obtained by applying the SVD technique to the matrix in Eq. (33). Once the eigenvalues are found, the associated mode shape can be obtained by substituting the corresponding boundary eigenvectors (i.e., eigenvectors for the boundary data) into the boundary integral equations for the domain point.

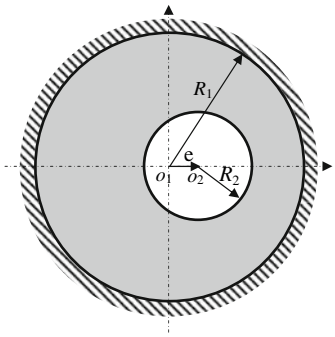

Case 1:
Geometric data:
R_1=1m
R_2=0.4m
e=0.0 ~ 0.5m
thickness=0.002m
Boundary condition:
Inner circle : free
Outer circle: clamped, simply -supported and free

Fig. 5 A circular plate with one circular hole

5 Spurious eigenvalue of multiply-connected plate eigenproblems and its remedy–SVD updating technique

For the 2-D multiply-connected problem [9,10], spurious eigenvalues occur when using BEM or BIEM even though the complex-valued kernel function is employed to solve the eigenproblem. This may cause the present method to obtain the additional spurious solutions. Therefore, SVD updating technique is adopted to suppress the appearance of spurious eigenvalue. The concept of this technique is to provide sufficient constrains to overcome the rank deficiency of the system.

The approach to suppress the appearance of spurious frequency is the criterion of satisfying all Eqs. (17)–(20) at the same time. Consider the circular plate with an eccentric hole and the outer clamped boundary and inner free boundary. Eqs. (30) and (31) reduce to

$$\begin{bmatrix} -U^{11} & \Theta^{11} & -M^{12} & V^{12} \\ -U_\theta^{11} & \Theta_\theta^{11} & -M_\theta^{12} & V_\theta^{12} \\ -U^{21} & \Theta^{21} & -M^{22} & V^{22} \\ -U_\theta^{21} & \Theta_\theta^{21} & -M_\theta^{22} & V_\theta^{22} \end{bmatrix}_{4N \times 4N} \begin{Bmatrix} v^1 \\ m^1 \\ \theta^2 \\ u^2 \end{Bmatrix}_{4N \times 1} = \begin{Bmatrix} 0 \\ 0 \\ 0 \\ 0 \end{Bmatrix}_{4N \times 1}. \tag{38}$$

Similarly, Eqs. (30) and (32) yield

$$\begin{bmatrix} -U^{11} & \Theta^{11} & -M^{12} & V^{12} \\ -U_m^{11} & \Theta_m^{11} & -M_m^{12} & V_m^{12} \\ -U^{21} & \Theta^{21} & -M^{22} & V^{22} \\ -U_m^{21} & \Theta_m^{21} & -M_m^{22} & V_m^{22} \end{bmatrix}_{4N\times 4N} \begin{Bmatrix} v^1 \\ m^1 \\ \theta^2 \\ u^2 \end{Bmatrix}_{4N\times 1} = \begin{Bmatrix} 0 \\ 0 \\ 0 \\ 0 \end{Bmatrix}_{4N\times 1}. \tag{39}$$

To obtain an overdetermined system, we can combine Eqs. (38) and (39) by using the SVD technique of updating terms as shown below:

$$\begin{bmatrix} -U^{11} & \Theta^{11} & -M^{12} & V^{12} \\ -U_\theta^{11} & \Theta_\theta^{11} & -M_\theta^{12} & V_\theta^{12} \\ -U^{21} & \Theta^{21} & -M^{22} & V^{22} \\ -U_\theta^{21} & \Theta_\theta^{21} & -M_\theta^{22} & V_\theta^{22} \\ -U^{11} & \Theta^{11} & -M^{12} & V^{12} \\ -U_m^{11} & \Theta_m^{11} & -M_m^{12} & V_m^{12} \\ -U^{21} & \Theta^{21} & -M^{22} & V^{22} \\ -U_m^{21} & \Theta_m^{21} & -M_m^{22} & V_m^{22} \end{bmatrix}_{8N\times 4N} \begin{Bmatrix} v^1 \\ m^1 \\ \theta^2 \\ u^2 \end{Bmatrix}_{4N\times 1} = \begin{Bmatrix} 0 \\ 0 \\ 0 \\ 0 \\ 0 \\ 0 \\ 0 \\ 0 \end{Bmatrix}_{8N\times 1}, \tag{40}$$

Eq. (40) can filter out spurious eigenvalues.

6 Numerical results and discussions

Natural frequencies and modes for circular plates with circular holes are determined by using the present method and FEM using the ABAQUS for comparison. In all cases, the inner boundary is subject to the free boundary condition. The thickness of plate is 0.002 m and the Poisson ratio $\nu = 1/3$. The general-purpose shell elements with reduced integration, S4R, of ABAQUS were used to model the plate problem. Although the thickness of the plate is 0.002 m, these elements do not suffer from transverse shear locking based on the theoretical manual of ABAQUS [1].

6.1 A circular plate with one circular hole [18,20,25,27]

A circular plate with one circular hole where the center is located along a radial axis from 0.0 to 0.5 m is considered to see the effect on true and spurious eigenvalues as shown in Fig. 5. The outer and inner radii are 1 m ($R_1 = 1$ m), and 0.4 m ($R_2 = 0.4$ m), respectively.

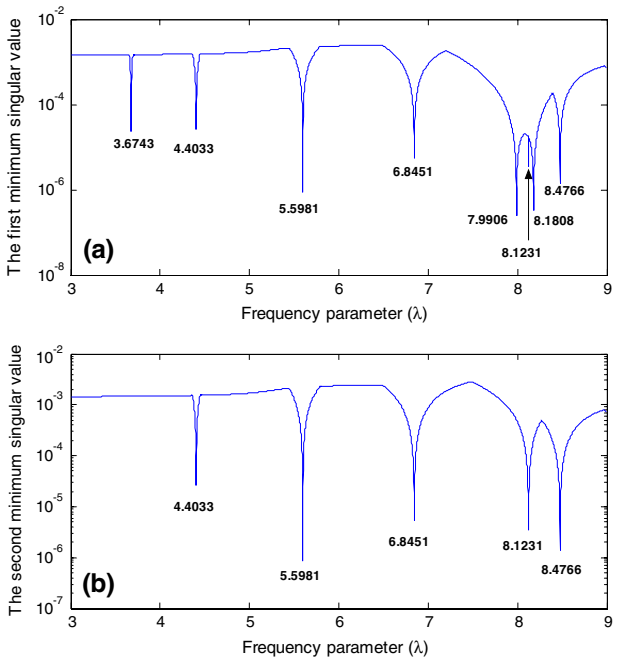

Fig. 6 The first and second minimum singular values versus the frequency parameter for the clamped-free annular plate ($R_1 = 1.0$, $R_2 = 0.4$ and $e = 0.0$)

6.1.1 A circular plate with the eccentricity of $e/R_1 = 0$

When the eccentricity equals to zero, this concentric case, i.e., annular plate, has the configuration of axial symmetry. Figure 6a, b shows the first and the second minimum singular values of the influence matrix of Eq. (33) versus the frequency parameter λ. Since the direct-searching scheme is used, the drop location indicates possible eigenvalues (true and spurious). The simultaneous appearance of drop indicates the multiplicities, e.g., 4.4033, as given in Fig. 6b. Figure 7 shows the first seven eigenvalues and eigenmodes. Values of m and n in the mode type M (m, n) are numbers of diametrical nodal lines and circular nodal lines, respectively. Diametrical node locates on a diametrical nodal line while circular node locates on a circular nodal line. In this case, the repeated eigenvalues always occur due to the axial symmetry. The corresponding mode shape has the same number of diametrical nodal lines, which can be rotated by an angle with respect to each other. From the convergence analysis, the required number of Fourier series of the present method equals to that of diametrical nodal lines of the mode considered due to its analytical nature. Consequently, only four terms ($M = 4$) in the Fourier series is sufficient to capture the first seven modes. In this case, 7788 elements and 8008 nodes were used to generate the corresponding FEM model.

Mode No.	1	2	3	4	5	6	7
Frequency parameter	3.6743	4.4033	4.4033	5.5981	5.5981	6.8451	6.8451
Mode type	M(0,0)	M(1,0)	M(1,0)	M(2,0)	M(2,0)	M(3,0)	M(3,0)
Mode shape using the present method	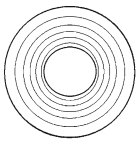	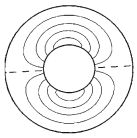	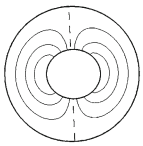	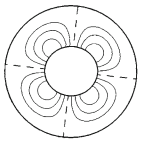	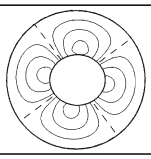	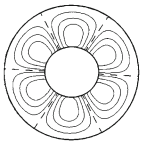	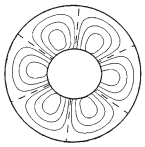
Frequency parameter	3.6738	4.4034	4.4034	5.6001	5.6001	6.8498	6.8498
Mode type	M(0,0)	M(1,0)	M(1,0)	M(2,0)	M(2,0)	M(3,0)	M(3,0)
Mode shape using ABAQUS	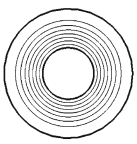	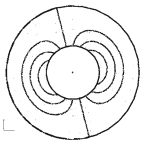	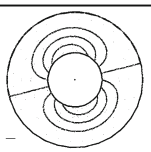	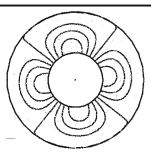	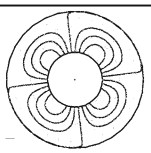	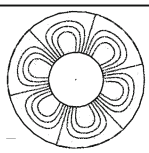	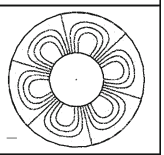

Fig. 7 The first seven natural frequency parameters, mode types and mode shapes for the clamped-free annular plate by using the present method and FEM ($R_1 = 1.0$, $R_2 = 0.4$ and $e = 0.0$)

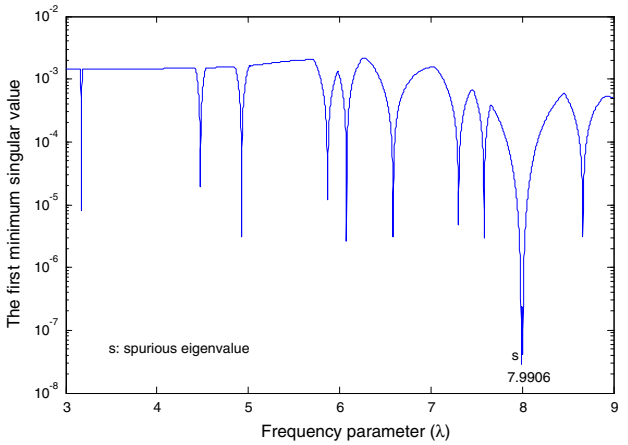

Fig. 8 The minimum singular value versus the frequency parameter for the clamped-free annular-like plate ($R_1 = 1.0$, $R_2 = 0.4$ and $e = 0.5$)

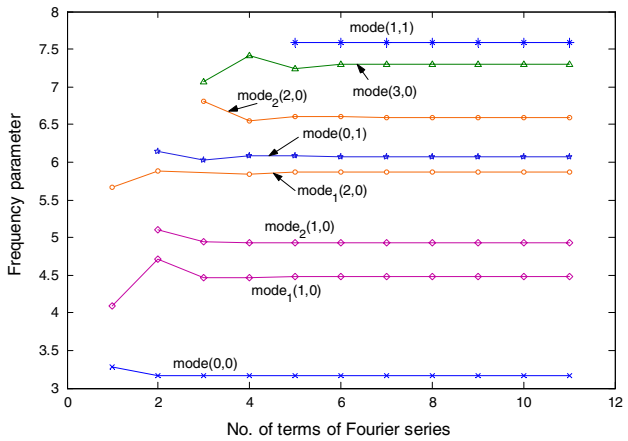

Fig. 9 Natural frequency parameter versus the number of terms of Fourier series for the clamped-free annular-like plate ($R_1 = 1.0$, $R_2 = 0.4$ and $e = 0.5$)

Comparing the numbers of unknowns and equations, it is obvious that the present method has a better computational efficiency than FEM does. Table 1 shows the first eight natural frequency parameters by using several methods. It is shown that the natural frequency parameters obtained by the present method are same as the analytical solutions up to four digits. By the way, the additional terms of the Fourier series play the role to determine which mode appears and not to affect its corresponding eigenvalue within four digits. Specifically, with only one term ($M = 1$), the present method can predict well the eigenvalues of mode (0, 0), mode (0, 1), mode (1, 0) and mode (1, 1). The main reason is the analytical nature of our method.

6.1.2 A circular plate with the eccentricity of $e/R_1 = 0.5$

When the center of circular hole is shifted along x-axis to 0.5 m from the center of outer circle, the significant changes in natural frequency and mode shape are examined here. Figure 8 indicates the minimum singular value of the influence matrix versus the frequency parameter λ using ten terms of Fourier series ($M = 10$). The multiplicity is only one due to the lack of axial symmetry. For the first eight eigenmodes, Fig. 9 shows the required number of terms of Fourier series to achieve the acceptable convergence of natural frequency parameter. For the mode $(m, 0)$ in Fig. 9, two corresponding modes are clearly distinguished by the subscript.

Table 1 The first eight natural frequency parameters (λ) for a clamped-free annular-like plate with the radius of $R_2/R_1 = 0.4$ and the eccentricity e/R_1 changing from 0.0 to 0.5 by using different methods

Eccentricity	Method[a]	1	2	3	4	5	6	7	8
$e/R_1 = 0.0$	1	3.6743	4.4033	4.4033	5.5981	5.5981	6.8451	6.8451	8.1231
	2	3.6738	4.4034	4.4034	5.6001	5.6002	6.8498	6.8500	8.1307
	3	3.6743	4.4033	4.4033	5.5981	5.5981	N/A	N/A	N/A
	4	3.6743	4.4033	4.4033	5.5981	5.5981	6.8451	6.8451	8.1231
$e/R_1 = 0.1$	1	3.5981	4.4071	4.5638	5.6304	5.6351	6.8610	6.8617	7.4873
	2	3.5979	4.4073	4.5639	5.6325	5.6373	6.8665	6.8665	7.4926
	3	3.6122	N/A	4.5854	N/A	5.6527	6.8725	N/A	N/A
$e/R_1 = 0.2$	1	3.4624	4.4180	4.8946	5.7182	5.8140	6.8495	6.9217	6.9414
	2	3.4624	4.4184	4.8951	5.7201	5.8158	6.8535	6.9260	6.9457
	3	3.4763	N/A	4.9141	N/A	5.8522	6.5264	N/A	N/A
$e/R_1 = 0.3$	1	3.3397	4.4342	5.0938	5.8223	6.2441	6.4615	7.0523	7.1270
	2	3.3398	4.4349	5.0952	5.8235	6.2459	6.4645	7.0556	7.2200
	3	3.3527	N/A	5.1063	N/A	6.2588	6.4565	N/A	N/A
$e/R_1 = 0.4$	1	3.2428	4.4539	5.0684	5.8784	6.1638	6.5758	7.2259	7.6069
	2	3.2431	4.4549	5.0699	5.8796	6.1667	6.5789	7.2291	7.6138
	3	3.2554	N/A	5.0809	N/A	6.1729	6.6194	N/A	N/A
$e/R_1 = 0.5$	1	3.1721	4.4753	4.9281	5.8689	6.0762	6.5875	7.3031	7.5835
	2	3.1723	4.4765	4.9293	5.8704	6.0797	6.5915	7.3079	7.5903
	3	3.1847	N/A	4.9428	N/A	6.0881	6.6494	N/A	N/A

The mesh sizes of FEM model for the eccentricity in the range of $e/a = 0.0$ to 0.5 are (8008, 7788), (8122, 7902), (8068, 7848), (7812, 7596), (7890, 7676) and (7828, 7618), respectively, where the data in the brackets denote the number of node and element for the FEM model

[a] Methods 1, 2, 3 and 4 denote the present method, FEM using ABAQUS, Laura [20,25] and Leissa [18] (analytical method), respectively

Mode No.	1	2	3	4	5	6	7
Frequency parameter	3.1721	4.4753	4.9281	5.8689	6.0762	6.5875	7.3031
Mode type	M(0,0)	M(1,0)	M(1,0)	M(2,0)	M(0,1)	M(2,0)	M(3,0)
Mode shape using the present method	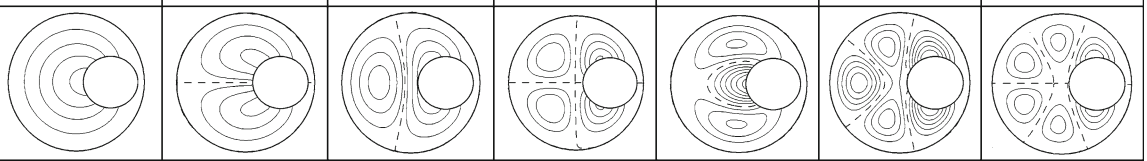						
Frequency parameter	3.1725	4.4768	4.9295	5.8709	6.0799	6.5920	7.3085
Mode type	M(0,0)	M(1,0)	M(1,0)	M(2,0)	M(0,1)	M(2,0)	M(3,0)
Mode shape using ABAQUS	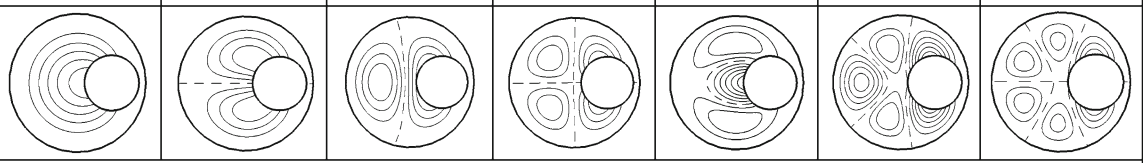						

Fig. 10 The first seven natural frequency parameters, mode types and mode shapes for the clamped-free annular-like plate by using the present method and FEM ($R_1 = 1.0$, $R_2 = 0.4$ and $e = 0.5$)

Subscript 1 denotes the straight diametrical nodal line, while subscript 2 denotes the curved diametrical nodal line. Not only do the appearances of eigenmodes not follow the rules for the concentric case as stated above, but also the more the number of the Fourier series terms is, the more accurate the natural frequency parameter is. From the convergence analysis, eight terms of the Fourier series are required to capture the first eight eigenmodes. Figure 10 shows the first seven

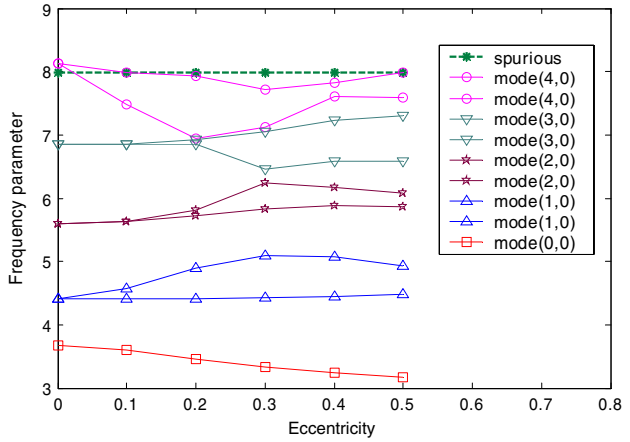

Fig. 11 Effect of the eccentricity e on the natural frequency parameter for the clamped-free annular-like plate ($R_1 = 1.0$, $R_2 = 0.4$)

eigenvalues and eigenmodes by using the present method and FEM and indicates excellent agreement in this eccentric case.

6.1.3 *Effect of eccentricity on the true and spurious eigensolutions*

The effect of eccentricity of e/R_1 on the frequency parameter is shown in Fig. 11. It shows that the repeated frequencies occurring in the annular case are gradually separated into two different values, e.g., mode$_1$ (1,0) (straight nodal line) and mode$_2$ (1,0) (curved nodal line), as the eccentricity increases due to the loss of original axial symmetry. From viewing Fig. 9, the mode (1,1) falls into the first eight eigenmodes when the eccentricity increases. This indicates that a large eccentricity decrease the radial stiffness for the circular mode. True eigenvalues depends on the eccentricity. However, the spurious eigenvalue (7.9906) is always there and independent of the eccentricity. This finding indicates that spurious eigenvalues are independent of the eccentricity but depends on the radius of inner circle. In summary, the eccentricity causes not only the separation of multiple eigenvalues but also the appearing sequence of mode types.

6.1.4 *Effect of boundary conditions on spurious eigenvalues and their remedy*

The case of eccentricity $e/R_1 = 0.2$ and three different boundary conditions ((a) clamped-free, (b) simply supported-free and (c) free-free) are considered here. By using three different methods ($U\Theta$, UM and SVD updating formulation), the minimum singular value of the influence matrix versus the frequency parameter λ is shown in Fig. 12. Three types of line, dash-dot, dot and solid, are used to represent the results for the $U\Theta$, UM and SVD updating formulation,

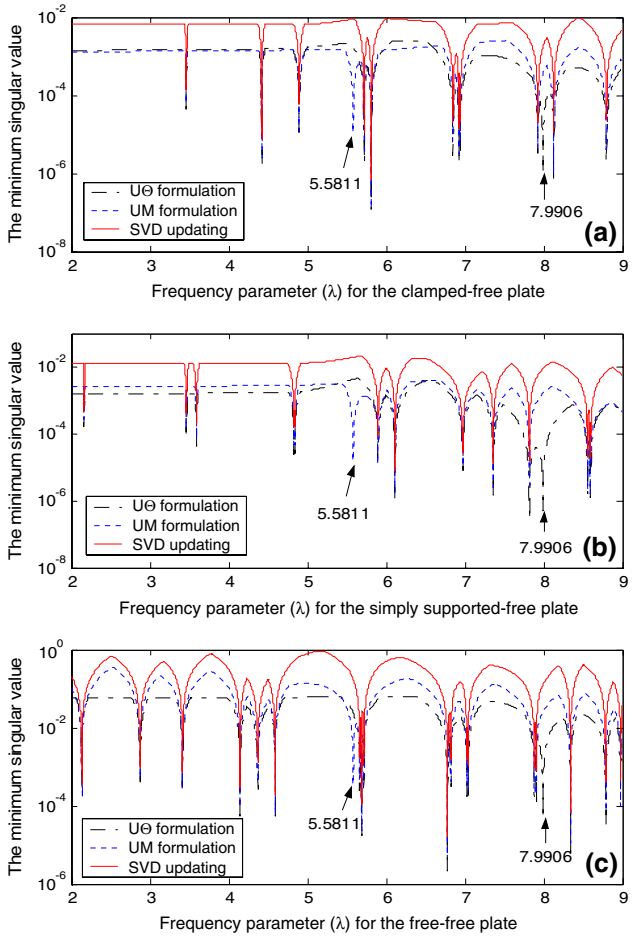

Fig. 12 The minimum singular value versus the frequency parameter by using three different methods ($U\Theta$,UM and SVD updating formulation) under three kind of boundary conditions (**a** clamped-free, **b** simply supported-free, **c** free-free)

respectively, in the same figure for comparison. The $U\Theta$ formulation means that both Eqs. (30) and (31) are used to construct the influence matrix of Eq. (33) in the boundary integral formulation. Similarly, the UM formulation adopted both Eqs. (30) and (32). Figure 12 indicates that the spurious eigenvalue (7.9906) is independent of the specified boundary condition and its value happens to be the true eigenvalue of circular clamped plate with a radius of 0.4 m. When the UM formulation is applied to solve the same problem, similar results are given except for the spurious eigenvalue (5.5811) which just equals to the true eigenvalue of simply-supported circular plate with a radius of 0.4 m. The numerical result shows that the occurrence of spurious eigenvalue depends on the size of the circular hole and the formulation employed. The specified type of boundary condition and the location of the center of the hole (i.e., eccentricity) can not change spurious eigenvalues. Figure 12 also shows that the SVD updating technique can successfully suppress the appearance of spurious eigenvalue and the present method can obtain

Table 2 The first eight frequency parameters (λ) for a simply supported-free annular-like plate with the radius of $R_2/R_1 = 0.4$ and the eccentricity e/R_1 changing from 0.0 to 0.5 by using different methods

Eccentricity	Method[a]	1	2	3	4	5	6	7	8
$e/a = 0.0$	1	2.1780	3.4506	3.4506	4.8060	4.8060	6.1049	6.1049	6.8777
	2	2.1780	3.4510	3.4510	4.8078	4.8079	6.1085	6.1085	6.8814
	3	2.1780	3.4506	3.4506	4.8060	4.8060	N/A	N/A	N/A
	4	2.1780	3.4506	3.4506	4.8060	4.8060	6.1049	6.1049	6.8777
$e/a = 0.1$	1	2.1747	3.4537	3.4859	4.8122	4.8126	6.1056	6.1056	6.3851
	2	2.1747	3.4542	3.4863	4.8141	4.8145	6.1093	6.1093	6.3878
	3	2.1791	N/A	3.5004	N/A	4.8185	6.1068	6.1068	N/A
$e/a = 0.2$	1	2.1657	3.4629	3.5894	4.8290	4.8370	5.8969	6.1110	6.1141
	2	2.1657	3.4634	3.5899	4.8307	4.8387	5.8991	6.1142	6.1176
	3	2.1693	N/A	3.6040	N/A	4.8484	5.9587	N/A	N/A
$e/a = 0.3$	1	2.1530	3.4775	3.7433	4.8501	4.9036	5.5672	6.1320	6.1463
	2	2.1531	3.4779	3.7436	4.8514	4.9050	5.5692	6.1351	6.1496
	3	2.1553	N/A	3.7571	N/A	4.9279	5.5801	N/A	N/A
$e/a = 0.4$	1	2.1393	3.4961	3.8790	4.8654	5.0682	5.3981	6.1819	6.2796
	2	2.1394	3.4966	3.8794	4.8663	5.0691	5.4003	6.1845	6.2823
	3	2.1404	N/A	3.8886	N/A	5.1045	5.4048	N/A	N/A
$e/a = 0.5$	1	2.1271	3.5163	3.9060	4.8639	5.2061	5.4315	6.2404	6.6531
	2	2.1272	3.5170	3.9067	4.8649	5.2080	5.4337	6.2430	6.6563
	3	2.1274	N/A	3.9128	N/A	5.2272	5.4424	N/A	N/A

The mesh sizes of FEM model for the eccentricity in the range of $e/a = 0.0$ to 0.5 are (8008, 7788), (8122, 7902), (8068, 7848), (7812, 7596), (7890, 7676) and (7828, 7618), respectively, where the data in the brackets denote the number of node and element for the FEM model

[a] Methods 1, 2, 3 and 4 denote the present method, FEM using ABAQUS, Laura [20,25] and Leissa [18] (analytical method), respectively

very accurate semi-analytic solutions as listed in Tables 1, 2 and 3.

6.1.5 Discussions of accuracy

The obtained eigenvalues using FEM of ABAQUS in Tables 1, 2 and 3 are greater than the other data except for the first eigenvalue of plate with eccentricities of 0.0 and 0.1 listed in Table 1. The effects of the mesh size of FEM model on the frequency parameter for the annular plate subject to clamped-free boundary condition are shown in Table 4. It is found that the first eigenvalue approaches the exact solution from the lower direction but the other eigenvalue approaches the exact solution from the upper direction when the mesh of FEM model is refined. But some eigenvalues decrease down the exact solution when the mesh size of FEM model still increases. For the sixth eigenvalue of the eccentricity $e/R_1 = 0.2$ shown in Table 1, the Laura's data is significantly different from the other results when a careful comparison is carried out. For this case, the mesh of FEM model is refined to see the tendency of this eigenvalue. This eigenvalue changes from 6.8535 to 6.8514 when the number of elements increases from 7788 to 13732. Furthermore, when the number of elements eventually increasing to 29948, the corresponding eigenvalue changes to 6.8498 which is very close to 6.8495 predicted by using the present method. In general, the results of the present method match better with those of ABAQUS than those of the Laura's method. The same trend can be observed from Tables 2 and 3 when different boundary conditions are considered. To our knowledge, the present method yields more accurate eigensolutions for the circular plate with an eccentric circular hole so far.

6.2 A circular plate with three circular holes

In order to demonstrate the generality of the present method, a circular plate with three holes is considered as shown in Fig. 13. The radii of holes are 0.4, 0.2 and 0.2 m and the coordinates of the center are (0.5 m, 0), (−0.3 m, 0.4 m) and (−0.3 m, −0.4 m), respectively, in the coordinate system with the origin at the center of outer circle. By using the *UM* formulation and eight terms of Fourier series ($M = 8$), the minimum singular value of the influence matrix versus the frequency parameter λ is shown in Fig. 14. The spurious eigenvalue of 5.5811 occurs when using the *UM* formulation and it is found to be the true eigenvalue of a clamped circular plate with a radius of 0.4 m. The spurious eigenvalues of the whole plate with three holes equal to the true eigenvalues of circular plate with the radius of inner holes. The smaller the radius is, the higher the eigenvalue is. So the spu-

Table 3 The first eight frequency parameters (λ) for a free-free annular-like plate with the radius of $R_2/R_1 = 0.4$ and the eccentricity e/R_1 changing from 0.0 to 0.5 by using different methods

Eccentricity	Method	1	2	3	4	5	6	7	8
e/a=0.0	1	2.1290	2.1290	2.9242	3.4301	3.4301	4.1283	4.1283	4.6110
	2	2.1291	2.1291	2.9242	3.4307	3.4307	4.1287	4.1287	4.6124
	3	2.1290	2.1290	2.9242	N/A	N/A	4.1283	4.1283	N/A
	4	2.1290	2.1290	2.9242	3.4301	3.4301	4.1283	4.1283	4.6110
e/a=0.1	1	2.1303	2.1304	2.9099	3.4260	3.4260	4.1322	4.1924	4.6051
	2	2.1304	2.1305	2.9099	3.4265	3.4265	4.1328	4.1929	4.6064
e/a=0.2	1	2.1342	2.1354	2.8745	3.4143	3.4144	4.1439	4.3690	4.5881
	2	2.1343	2.1355	2.8746	3.4149	3.4150	4.1445	4.3697	4.5894
e/a=0.3	1	2.1406	2.1471	2.8327	3.3972	3.3983	4.1626	4.5569	4.5627
	2	2.1407	2.1472	2.8329	3.3976	3.3988	4.1633	4.5580	4.5639
e/a=0.4	1	2.1488	2.1718	2.7969	3.3772	3.3843	4.1876	4.5291	4.5327
	2	2.1489	2.1719	2.7971	3.3777	3.3847	4.1885	4.5299	4.5341
e/a=0.5	1	2.1566	2.2225	2.7795	3.3552	3.3948	4.2175	4.5010	4.5093
	2	2.1568	2.2224	2.7798	3.3561	3.3940	4.2186	4.5040	4.5067

* Methods 1, 2, 3 and 4 denote the present method, FEM using ABAQUS, Laura [27] and Leissa [28] (analytical method), respectively.
The mesh sizes of FEM model for the eccentricity in the range of e/a=0.0 to 0.5 are (8008, 7788), (8122, 7902), (8068, 7848), (7812, 7596), (7890, 7676) and (7828, 7618), respectively, where the data in the brackets denote the number of node and element for the FEM model

Table 4 The effect of mesh size of FEM model on the frequency parameter for clamped-free annular plate with condition ($R_1 = 1.0$, $R_2 = 0.4$)

Mode no.	(8008,7788)[a]	(13755,13462)	(29444,29005)	Exact
1	3.6738	3.6741	3.6742	3.6743
2	4.4034	4.4031	4.4028	4.4033
3	4.4034	4.4031	4.4028	4.4033
4	5.6001	5.5991	5.5982	5.5981
5	5.6002	5.5991	5.5982	5.5981
6	6.8498	6.8477	6.8460	6.8451
7	6.8500	6.8477	6.8460	6.8451
8	8.1307	8.1274	8.1250	8.1231

[a] The mesh size of FEM model denotes (no. of node, no. of element)

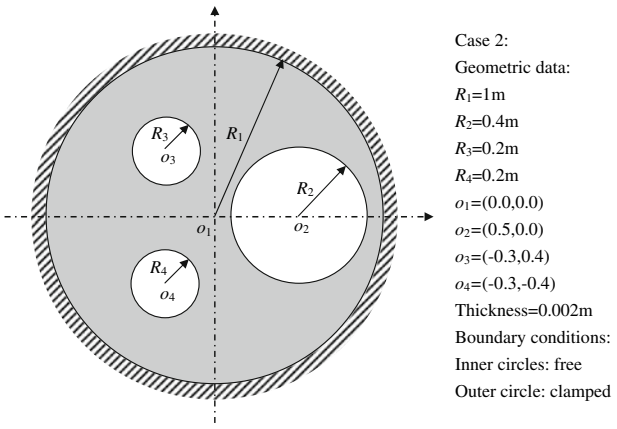

Fig. 13 A circular plate with three circular holes

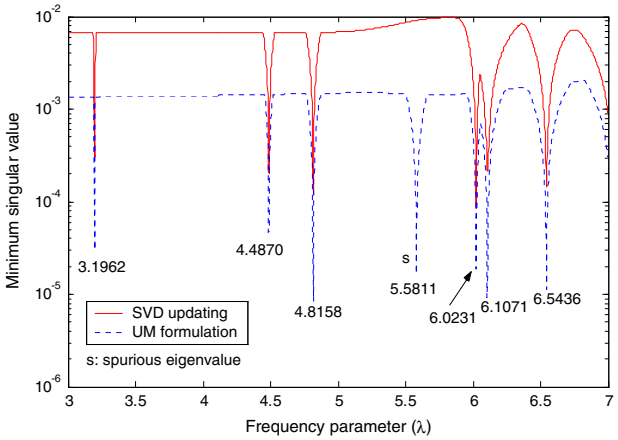

Fig. 14 The minimum singular value versus the frequency parameter by using the UM formulation and the SVD updating technique for a circular clamped plate with three circular free holes ($R_1 = 1.0$, $R_2 = 0.4$, $R_3 = 0.2$ and $R_4 = 0.2$)

rious eigenvalues corresponding to inner circle of the minimum radius 0.2 m are too large to appear in the range of λ in Fig. 14. It also demonstrates that the spurious eigenvalue can be filtered out by using the SVD updating technique. The same problem is also solved by using ABAQUS. The numbers of node and element of FEM model are 7570 and 7296, respectively. After Comparing with the present method, the high efficiency can also be observed for this case. Figure 15 shows the first six natural frequency parameters and modes by using ABAQUS and the present method. Excellent agreement between the results of the present method and those of ABAQUS is observed.

7 Concluding remarks

A semi-analytical approach for solving the natural frequencies and modes of the circular plate with multiple circular

MODE	1	2	3	4	5	6
Present method	3.1962	4.4870	48158	6.0231	6.1071	6.5436
	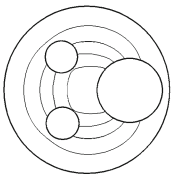	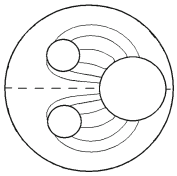	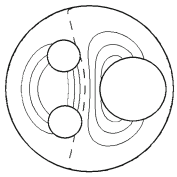	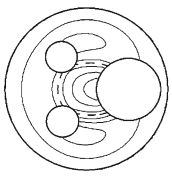	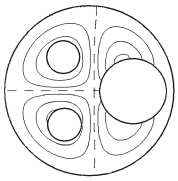	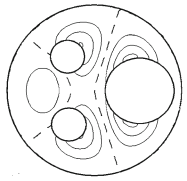
ABAQUS	3.1967	4.4886	4.8178	6.0270	6.1080	6.5466
	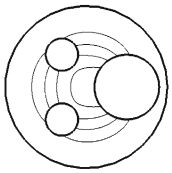	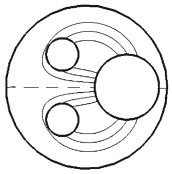	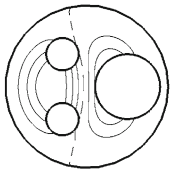	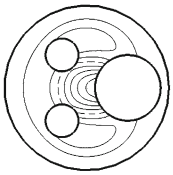	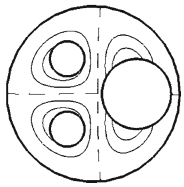	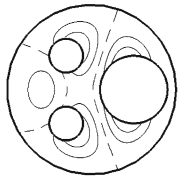

Fig. 15 The first six natural frequency parameters and mode shapes for a circular clamped plate with three circular free holes by using the present method and FEM ($R_1 = 1.0$, $R_2 = 0.4$, $R_3 = 0.2$ and $R_4 = 0.2$)

holes was proposed. Natural frequencies and modes were determined by employing the null-field integral formulation in conjunction with degenerate kernels, tensor rotation and Fourier series. The improper integrals in the null-field integral formulation were avoided by using the degenerate kernels and were easily calculated through the series sum. For the non-concentric general case, the rotated degenerate kernels have been derived on the adaptive observer system. Once the Fourier coefficients of boundary densities have been determined, the corresponding mode shape can be obtained by using the boundary integral equations for domain points. The effects of eccentricity of the hole and type of boundary condition on true and spurious eigenvalues are examined. The natural frequencies and mode shapes for multiply-connected plate problems with multiple circular holes have been solved easily and efficiently by using the present method in comparison with the available approximate analytic solutions and FEM results using ABAQUS. Excellent agreement between the results of the present method and those of ABAQUS is observed. The value of spurious eigenvalue depends on the radius of the inner hole and the formulation. The specified boundary condition and the location of the hole influence the true eigenvalue. Finally, the SVD technique of updating terms can successfully suppress the appearance of spurious eigenvalue and the present method can obtain very accurate semi-analytic solutions. To avoid the contamination of spurious eigenvalues, we recommend the SVD updating technique to obtain all the eigenvalues instead of SVD only in real computation. As can be seen from the numerical results, the present method provides more accurate semi-analytic eigensolutions for the circular plate with an eccentric circular hole or multiple holes so far.

References

1. ABAQUS 6.5 (2004) Hibbitt, Karlsson and Sorensen Inc., RI
2. Chen JT, Lin SY, Chen IL, Lee YT (2006) Mathematical analysis and numerical study to free vibrations of annular plates using BIEM and BEM. Int J Numer Meth Eng 65:236–263
3. Chen JT, Lin SY, Chen KH, Chen IL (2004) Mathematical analysis and numerical study of true and spurious eigenequations for free vibration of plates using real-part BEM. Comput Mech 34:165–180
4. Chen JT, Hong HK (1999) Review of dual boundary element methods with emphasis on hypersingular integrals and divergent series. Appl Mech Rev ASME 52(1):17–33
5. Chen JT, Shen WC, Wu AC (2006) Null-field integral equations for stress field around circular holes under anti-plane shear. Eng Ana Bound Elem 30:205–217
6. Chen JT, Hsiao CC, Leu SY (2006) Null-field integral equation approach for plate problems with circular holes. J Appl Mech ASME 73:679–693
7. Chen JT, Shen WC, Chen PY (2006) Analysis of circular torsion bar with circular holes using null-field approach. Comput Model Eng Sci 12(n2):109–119
8. Chen JT, Chen CT, Chen PY, Chen IL (2007) A semi-analytical approach for radiation and scattering problems with circular boundaries. Comput Methods Appl Mech Eng 196:2751–2764
9. Chen JT, Lin JH, Kuo SR, Chyuan SW (2001) Boundary element analysis for the Helmholtz eigenvalue problems with a multiply connected domain. Proc R Soc Lond A 457:2521–2546
10. Chen JT, Liu LW, Hong H-K (2003) Spurious and true eigensolutions of Helmholtz BIEs and BEMs for a multiply-connected problem. Proc R Soc Lond A 459:1891–1924
11. Cheng L, Li YY, Yam LH (2003) Vibration analysis of annular-like plates. J Sound Vib 262:1153–1170
12. Gradshteyn IS, Ryzhik IM (1996) Table of integrals, series, and products, 5th edn. Academic Press, New York
13. Hutchinson JR (1991) Analysis of plates and shells by boundary collocation. In: Beskos DE (ed) Boundary elements analysis of plates and shells. Springer, Berlin pp 314–368
14. IMSL Math (1999) Library Volumes 1 and 2 Version 4.01 Visual Numerics Inc.

15. Kress R (1989) Linear integral equations. Springer, New York
16. Kitahara M (1985) Boundary integral equation methods in eigenvalue problems of elastodynamics and thin plates. Elsevier, Amsterdam
17. Khurasia HB, Rawtani S (1978) Vibration analysis of circular plates with eccentric hole. ASME J Appl Mech 45:215–217
18. Leissa W (1969) Vibration of plates. NASA SP-160
19. Leissa W, Narita Y (1980) Natural frequencies of simply supported circular plates. J Sound Vib 70:221–229
20. Laura PAA, Masia U, Avalos DR (2006) Small amplitude, transverse vibrations of circular plates elastically restrained against rotation with an eccentric circular perforation with a free edge. J Sound Vib 292:1004–1010
21. Providatis CP, Beskos DE (1999) Dynamic analysis of plates by boundary elements. ASME Appl Mech Rev 52(7):213–236
22. Reddy JN (2004) Mechanics of laminated composite plates and shells: theory and analysis. CRC Press, Boca Raton, FL
23. Tanaka M, Sladek V, Sladek J (1994) Regularization techniques applied to boundary element methods. Appl Mech Rev 47:457–499
24. Vogel SM, Skinner DW (1965) Natural frequencies of transversely vibrating uniform annular plates. ASME J Appl Mech 32:926–931
25. Vega DA, Vera SA, Sanchez MD, Laura PAA (1998) Transverse vibrations of circular, annular plates with a free inner boundary. J Acoustical Soc Am 103:1225–1226
26. Vera SA, Sanchez MD, Laura PAA, Vega DA (1998) Transverse vibrations of circular, annular plates with several combinations of boundary conditions. J Sound Vib 213(4):757–762
27. Vera SA, Laura PAA, Vega DA (1999) Transverse vibrations of a free-free circular annular plates. J Sound Vib 224(2):379–383
28. Wong WO, Yam LH, Li YY, Law LY, Chan KT (2000) Vibration analysis of annular plates using mode subtraction method. J Sound Vib 232(4):807–822
29. Wu CS (2004) Degenerate scale analysis for membrane and plate problems using the meshless method and boundary element method. Master thesis, National Taiwan Ocean University, Keelung